03,12

Ab initio calculations of electronic properties, frequency dispersion of dielectric coefficients and the edge of the optical absorption of $TlInS_2\langle Sn\rangle$ single crystals

© S.N. Mustafaeva[1], M.M. Asadov[2,3], S.S. Huseynova[1], N.Z. Hasanov[1], V.F. Lukichev[4]

[1]Institute of Physics, Azerbaijan National Academy of Sciences,
Baku, Azerbaijan
[2] Nagiev Institute of Catalysis and Inorganic Chemistry, Azerbaijan National Academy of Sciences,
Baku, Azerbaijan
[3] Research Institute of Geotechnological Problems of Oil, Gas and Chemistry, ASUOI,
Baku, Azerbaijan
[4] Valiev Institute of Physics and Technology, Russian Academy of Sciences
Moscow, Russia

E-mail: solmust@gmail.com

Received February 27, 2022
Revised February 27, 2022
Accepted March 10, 2022

Calculations of the band structure and density of states for supercells of $TlInS_2$ and $TlInS_2\langle Sn\rangle$ semiconductor crystals with monoclinic singony within the density functional theory (DFT) are presented. In DFT calculations, the Coulomb repulsion (the Hubbard parameter (U)) was taken into account in order to correctly describe the band gap (E_g) of crystals. It is shown that the maximum of the valence band and the minimum of the conduction band of $TlInS_2$ are located at the center (point Γ) of the Brillouin zone, which points to the direct energy of the band gap of the $TlInS_2$ and $TlInS_2\langle Sn\rangle$ crystals. Thrue results of calculating the band structure and features of the distribution of the density of electronic states in $TlInS_2$ and $TlInS_2\langle Sn\rangle$ are discussed.

$TlInS_2$ single crystals doped with 0.1 mol.% tin ($TlInS_2\langle 0.1$ mol.% $Sn\rangle$) were synthesized and then grown by the Bridgman–Stockbarger method. The frequency dispersion of the dielectric coefficients and conductivity of a $TlInS_2$ and $TlInS_2\langle 0.1$ mol.% $Sn\rangle$ single crystals in the frequency range $f = 5 \cdot 10^4 - 3.5 \cdot 10^7$ Hz is studied. It is shown that relaxation losses occur in $TlInS_2\langle Sn\rangle$. A hopping mechanism of ac charge transfer in $TlInS_2\langle Sn\rangle$ has been established. In $TlInS_2\langle Sn\rangle$, the parameters of localized states, such as the density of states near the Fermi level and their energy spread, the average hopping time and distance, and the concentration of deep traps, are estimated.

The optical properties of $TlInS_2$ and $TlInS_2\langle 0.1$ mol.% $Sn\rangle$ single crystals have been studied.

The values of E_g for direct optical transitions in $TlInS_2$ and $TlInS_2\langle 0.1$ mol.% $Sn\rangle$ crystals were obtained from the optical absorption spectra. It has been shown that the introduction of 0.1 mol.% Sn, which replaces indium atoms, into $TlInS_2$ reduces the value of E_g, for example, at 150 K from 2.539($TlInS_2$) to 2.486 eV ($TlInS_2\langle 0.1$ mol.% $Sn\rangle$). From optical measurements, the average temperature coefficient of the band gap $\partial E_g/\partial T = -7 \cdot 10^{-4}$ eV/K for $TlInS_2\langle Sn\rangle$ was calculated. The decrease in the band gap of the $TlInS_2\angle Sn\rangle$ single crystal with respect to $TlInS_2$ is 16 meV at 300 K and 53 meV at 150 K.

Keywords: supercell, semiconductor $TlInS_2$, tin doping, monoclinic syngony, density functional theory, electronic structure, single crystals, dielectric properties, optical absorption, charge transfer, parameters of localized states.

DOI: 10.21883/PSS.2022.06.53823.299

1. Introduction

The thallium(I) indium(III) disulfide ($TlInS_2$) belongs to the ternary chalcogenide group $A^{III}B^{III}C_2^{VI}$ with a lamellar structure. The crystals of this group are characterized by their semiconductor and ferroelectric properties [1]. The structure of the $TlInS_2$ compound is characterized by formation of several polymorphic modifications [2], thereby affecting their physical properties [3–6]. It is known that the following stable polymorphic modifications of the $TlInS_2$ compound exist — a monoclinic one [7,8], a rhombic one [7], a tetragonal one [9], a hexagonal one [10] and a triclinic one [11].

The $TlInS_2$ compound with the monoclinic crystal system, having a lamellar structure, is characterized by an anisotropy of the physical properties and is promising as a function material in various semiconductor devices. Since the $TlInS_2$ crystal structure is lamellar, and it forms several polymorphic modifications, the said features of the structure significantly affect the physical properties of $TlInS_2$ [7,8,12–15].

The $TlInS_2$ is a semiconductor of the *p*-type. Alloying the semiconductors with various impurities allows controlling the physical properties of the materials. In particular, the alloying of $TlInS_2$ with elements having a various number of valence electrons should lead to various impacts on the

physical properties of $TlInS_2$. For example, the paper [16] studies permittivity spectra and the electron paramagnetic resonance (EPR) of the $TlInS_2$ crystals alloyed by Fe within the temperature range of 5−300 K. It has shown significant decrease in the permittivity of $TlInS_2$ and a shape change of its temperature dependence as a result of impact of the alloyed iron atoms. It is established that the EPR lines exhibit noticeable splitting and there are evidently additional resonance lines at the temperatures below 200 K, which corresponds to the temperature of the ferroelectric phase transition.

The elastic and vibratory properties of the $TIInS_2$ and $TlIn(S_{0.75}Se_{0.25})_2$ crystals have been calculated in the paper [17] by using the DFT/PBE method with addition of the dispersion correction. It has calculated the elastic constants, the bulk modulus, the Young modulus, the shear modulus and the Poisson ratio. It has also calculated the phonon energy dispersion curves and the partial densities of the phonon states for $TIInS_2$ and $TlIn(S_{0.75}Se_{0.25})_2$. It is shown that the alloying strongly affects the crystal properties. Thus, for example, the Young modulus calculated for the $TlInS_2$ crystal is equal to 39.84 GPa, whereas for the $TlIn(S_{0.75}Se_{0.25})_2$ crystal it is almost three times less and equal to 14.95 GPa.

The purpose of the present paper — to investigate the electron structure, dielectric and optical properties of the $TlInS_2$ crystal, containing a tin substitution impurity. It has investigated the impact of tin (0.1 mol.% Sn) as a donor substitution impurity on the dielectric and optical characteristics of the grown $TlInS_2$ single crystals in the monoclinic crystal system and established a charge transfer mechanism in an alternating electrical fields of the radio frequency range.

When being incorporated into the $TlInS_2$ crystal lattice and substituting the indium atoms, the tin impurity having 4 valence electrons and an ion radius close to indium should lead to formation of the donor level near the conductivity band, thereby allowing, in particular, varying the band gap.

2. Calculation and experiment procedure

2.1. Calculation model and details

The band structure and the density of electron states have been calculated for the $TlInS_2$ lamellar semiconductor with the monoclinic crystal system. The ATK software package based on the density functional theory (DFT) was used [9]. The following electron configurations have been considered: Tl — $5d^{10}6s^26p^1$, In — $4d^{10}5s^25p^1$, S — $3s^23p^4$, Sn — $4d^{10}5s^25p^2$. The core electrons have been described by means of the Vanderbilt ultra-soft pseudopotentials. The $TlInS_2$ supercells containing 32 atoms and the impurities of Sn atoms have been used. The exchange-correlation functions was used in the local density approximation (LDA) and generalized gradient approximation (GGA) with PBE parametrization [18–21].

The lattice cell geometry of $TlInS_2$ and $TlInS_2\langle Sn\rangle$ have been pre-optimized. The structural optimization change included — positions of ions, a shape and volume of the cell. In the calculations of the self-consistent field, the flat wave cutoff energy was selected to ensure that divergence for the full (free) energy of the lattice cell is not worse than $5 \cdot 10^{-6}$ eV/atom and equal to 300 eV. (The divergence threshold for the interatomic forces was 10^{-4} eV/Å.) The net sample of Monkhorst–Pack k-points was established at the level of $4 \times 4 \times 2$ dots for the Brillouin zone. The band gap (E_g) of the $TlInS_2$-based crystals has been corrected taking into account a Hubbard parameter of Coulomb repulsion DFT + U [20,21].

2.2. Preparation of samples

***Synthesis of* $TlInS_2$.** The specially pure chemical elements Tl (Tl 00), In (In 00), S (ultra high purity 16−5) and Sn (99.99%) have been used as initial components for the synthesis of the $TlInS_2$ compound. $TlInS_2$ and the samples based there on $TlInS_2\langle 0.1$ mol.% Sn$\rangle$ have been synthesized by a single temperature method [20,22]. The chemical elements of stoichiometric ratios have melted in quartz ampules evacuated to 10^{-3} Pa, which were put inside an electric oven. At the initial stage, the ampules were heated up to 720 K at the rate of 20−30 K/h, to be held thereat during 24 h. Then ampules had been heated to 1100 K to be held thereat during 5 h. Then the samples were cooled to the room temperature at the rate of 10−20 K/h. The synthesized samples were homogenized in the vacuum of 10^{-3} Pa at 670 K during 120 h. After annealing the ampules with the alloys were quenched in cold water. Complete synthesis of the $TlInS_2$ and $TlInS_2\langle Sn\rangle$ polycrystallines, their homogeneity and uniqueness were controlled by the differential thermal analysis (DTA) and the X-ray diffraction analysis (XDA). The DTA was done on the STA 449 F3 Jupiter unit. The XDA of the $TlInS_2\langle Sn\rangle$ powder samples was carried out in the diffractometer of the D8-ADVANCE type at the mode $0.5° < 2\theta < 80°$ (CuK_α-radiation; $\lambda = 1.5418$ Å) at 40 kV and 40 mA.

***Growth of single crystals*.** The single crystals were grown from the pre-synthesized $TlInS_2$ and $TlInS_2\langle 0.1$ mol.% Sn$\rangle$ polycrystallines by the Bridgman–Stockbarger method [20,22]. The polycrystalline sample of the weight of 10 g was loaded into a growth quartz ampule of the length of 30 mm and the diameter of 9 mm (container) with a cone-shaped bottom, which was evacuated and soldered up. Then the ampule with the sample was put into a tubular vertical two-zone growth electric oven of the growth unit. The temperature of each of the two oven zones was controlled separately from each other. An accuracy of maintaining the temperature inside the two-zone oven was ±0.5 K. The temperature gradient at the crystallization front was 20 K/cm. The maximum temperature of the hot zone was 1050 K. The crystal growth rate was 0.1 mm/h. The sample in the container, which was put into the hot zone of the growth oven, had been

melt and held during 1−2 h. Then the melt ampule was transferred from the hot zone into the growth zone at the rate of 10 mm/day and the single crystals were grown. Then both oven zones had been simultaneously cooled at the rate of 20−30 K/h to 700 K and the single crystals had been annealed during 100 h. Then the annealed single crystals were cooled down to the room temperature. Thus, the homogeneous dark orange $TlInS_2$ and $TlInS_2\langle 0.1\,\text{mol.\% Sn}\rangle$ single crystals were produced.

2.3. Procedure of measurement of the properties

The dielectric coefficients of the $TlInS_2$ and $TlInS_2\langle 0.1\,\text{mol.\% Sn}\rangle$ single crystal samples were measured by the resonance method [20]. The range of alternating electric field frequencies was $5\cdot 10^4-3.5\cdot 10^7$ Hz.

For electric measurements, the $TlInS_2\langle \text{Sn}\rangle$ single crystal samples were made as flat condensers. Silver paste was used as electrodes. The thickness of the $TlInS_2\langle \text{Sn}\rangle$ single crystal samples was 0.03−0.07 cm. The dielectric properties were measured in a direction perpendicular to the crystal layers. All the dielectric measurements were carried out at 300 K. Reproducibility of the resonance position was ±0.2 pF in terms of capacitance, and ±1.0−1.5 of scale division in terms of quality factor ($Q = 1/\text{tn}\,\delta$). Thereat, the largest deviations from the average values were 3−4% for ε' and 7% for $\text{tn}\,\delta$.

The absorption coefficient (α) near the fundamental edge is determined by a zone dispersion and proportional to the state density. Moreover, the study of the spectrum distribution of the absorption coefficient allowed determining the band gap (E_g) of $TlInS_2\langle \text{Sn}\rangle$. The absorption coefficient was calculated as per transmission spectra near the edge of intrinsic absorption.

The samples for studying the optical absorption spectra were cleaved off the single crystal ingot of $TlInS_2\langle 0.1\,\text{mol.\% Sn}\rangle$ to be shaped as thin plates of the thickness of 20 to 90 μm. The light was directed to the $TlInS_2\langle \text{Sn}\rangle$ samples parallel to the crystal crystallographic axis c. The optical transmission spectra were studied by means of a laboratory unit based on the MDR-23 monochromator and the nitrogen cryostat. The FEU-100 was used as an emission receiver.

3. Results and discussion

3.1. Results of ab initio calculations

The *ab initio* calculations of the energy state of the solid bodies have to be taken to solve the quantum-mechanical equations for many particles ($\sim 10^{23}\,\text{cm}^3$ of electrons and ions, which is typical for solid bodies), which interact with each other. This problem for the multi-particle crystal of many freedom degrees is simplified by solving the Schr'dinger equation within formalism of the density functional theory [23]. The multi-electron wave function, which depends on $3N$ variables — along 3 spatial coordinates per each of N electrons, is replaced by a scalar electron density of the ground state $\rho(\mathbf{r} = \sum_{i=1}^{N}\phi_i^*(r)\phi_i(r)$. In this situation, the electron density is a function of the three spatial coordinates.

To describe systems including, for example, heavy metals and magnetic crystals, for a variable, besides the magnitude $\rho(\mathbf{r})$, the magnetization density vector $m(r)$ is also taken into account. That is, for correctness of the calculations, such systems shall include contribution by the spin-allowed (of a spin type) electron density $\rho^{\alpha\beta}(r)$, where the spin indices α and β accept two values: spin-up and spin-down ($\alpha^{\uparrow}, \beta_{\downarrow}$). Relation between the parameters $\rho(\mathbf{r})$, $\rho^{\alpha\beta}(r)$ and the vector $m(r)$ is determined by the expressions:

$$\rho(\mathbf{r}) = \sum_{\alpha}\rho^{\alpha\alpha}(r) = \sum_{i=1}^{N}\phi_{i\alpha}^*(r)\phi_{i\beta}(r), \tag{1}$$

$$m(r) = \sum_{\alpha\beta}\sigma^{\alpha\beta}\rho^{\alpha\beta}(r), \tag{2}$$

$$\rho^{\alpha\beta}(r) = \frac{1}{2}\left(\rho(r)\delta_{ij}^{\alpha\beta} + m_x(r)\sigma_x^{\alpha\beta} + m_y(r)\sigma_y^{\alpha\beta} + m_z(r)\sigma_z^{\alpha\beta}\right). \tag{3}$$

Here, the 2×2 matrix elements are indexed by α and β, where δ_{ij} — the Kronecker symbol; $\boldsymbol{\sigma} = \sigma_x, \sigma_y, \sigma_z$ is a vector consisting in the matrices:

$$\sigma_x = \begin{pmatrix} 0 & 1 \\ 1 & 0 \end{pmatrix},\ \sigma_y = \begin{pmatrix} 0 & -i \\ i & 0 \end{pmatrix},\ \sigma_z = \begin{pmatrix} 1 & 0 \\ 0 & -1 \end{pmatrix}. \tag{4}$$

The ground state density $\rho(\mathbf{r})$ determines mutually non-interacting electrons in the external potential $v_{ext}(r)$ of the nuclei of the system under study. That is, instead of the system with the big number of electrons in the external potential of the nuclei, DFT can deal with the electron density in a certain potential to simplify a calculation task.

It is accepted for the potential $v_{ext}(r)$ that there is a universal functional $F[\rho]$ of the electron density $\rho(\mathbf{r})$. At this, the potential $v_{ext}(r)$ is related to a minimum functional of the full energy $E_e[\rho]$. The ground state of the electron system for a gas of the interacting particles in the external potential $v_{ext}(r)$ at the equilibrium value $n(r)$ is specified by the energy potential:

$$E_e[\rho] = F[\rho] + \int v_{ext}(r)\rho(\mathbf{r})dr. \tag{5}$$

The universal functional is presented in the following form:

$$F[\rho] = T_0[\rho] + E_{\text{H}}[\rho] + E_{\text{XC}}[\rho], \tag{6}$$

where $T_0[\rho]$ — the kinetic energy of motion of the non-interacting electrons, $E_{\text{H}}[\rho]$ — the potential energy of mutual interaction of electrons or the Hartree energy, which describes static Coulomb interaction of the electron density, $E_{\text{XC}}[\rho]$ — the energy of exchange-correlation interaction of electrons.

Table 1. Parameters of the $TlInS_2$ crystal lattice with the monoclinic crystal system (sp.gr. $C2/c$), as obtained by using the exchange-correlation functions

Parameters of the lattice	DFT calculation				Experiment	
	LDA	GGA-PBE	SGGA-PBE	DFT(D) + U [24]	[7]	[11]
a, Å	10.9019	11.1468	10.952	7.783385	10.942	10.90
b, Å	10.9452	11.1594	10.957	7.783385	10.484	10.94
c, Å	15.1811	15.3783	15.177	15.267074	15.606	15.18
β°	96.883	96.883	96.883	96.882950	100.70	100.21
γ°				90.035269		

Table 2. Theoretical and experimental values of the band gap of the $TlInS_2$ and $TlInS_2\langle Sn\rangle$ single crystals

Composition	DFT calculation			Experiment		
	E_g, eV					
	SLDA	SGGA-PBE	DFT(D) + U [24]	150 K	300 K	295 K [25]
$TlInS_2$	1.2	2.49	2.296	2.539	2.399	2.403
$TlInS_2\langle Sn\rangle$	1.1	2.17		2.486	2.383	
$TlInS_2\langle Ag\rangle$						2.399

From the above equations for the energy potential we have:

$$E_0 = E_e[\rho] = T_0[\rho] + \int v_{ext}(r)\rho(\mathbf{r})dr + E_{\mathrm{H}}[\rho] + E_{\mathrm{XC}}[\rho] \quad (7a)$$

or

$$E_0 = E_e[\rho] = E_{\mathrm{kin}}[\rho] + E_{\mathrm{ion}}[\rho] + E_{\mathrm{Hartree}}[\rho] + E_{\mathrm{XC}}[\rho]. \quad (7b)$$

The exchange-correlation functional of the supercell has been calculated in the local density approximation for the homogeneous electron gas (LSDA) and the spin generalized gradient approximation (SGGA) taking into account the electron spin. I.e., the approximation of $E_{\mathrm{XC}}^{\mathrm{SLDA}}[n_\uparrow, n_\downarrow]$ was carried out, where the electron-electron interactions are taken into account in a simplified way, so was $E_{\mathrm{XC}}^{\mathrm{SGGA}}[n_\uparrow, n_\downarrow]$, wherein the spin polarization was taken into account.

The supercell of the unordered lattice based on $TlInS_2\langle Sn\rangle$ with the monoclinic crystal system was formed by creating a periodic structure of a big size. In this cell the atoms of the various kind occupy a certain position in the lattice, while the required concentration of the alloying element in the crystal is achieved by increasing the supercell size. Depending on the atomic configurations, it is possible to obtain different values of the lattice full energy.

The $TlInS_2\langle Sn\rangle$ supercell was modeled as a four-component crystal with the stoichiometric concentration of the atoms with the spin-up and the spin-down for each chemically nonequivalent component of the structure. The exchange and correlation effects were taken into account within the SGGA. The own values have been calculated for a basic set including the s, p and d-valence orbitals, by means of the low-energy (soft) nucleus approximation, wherein the nucleus states are calculated again after each iteration.

During alloying the semiconductors, the physical properties depend, in particular, on what position is occupied by an alloying additive within the crystal structure of the semiconductor. The $TlInS_2$ lamellar crystal can have indium partially substituted with tin. It is correlated to the structure features of the $TlInS_2$ ($Tl^+In^{3+}S_2^{2-}$), where each In^{3+} cation forms four covalence bonds with four S_2^{2-} adjacent anions, and to the fact that the ion radius of the alloying Sn^{4+} (0.69 Å) is closer to the ion radius of In^{3+} (0.80 Å) than to the ion radius of Tl^{1+} (1.50 Å).

Results of calculation of the lattice parameters and the band gap of the $TlInS_2$, $TlInS_2\langle Sn\rangle$ crystals are given in Tables 1 and 2. The lattice parameters as calculated by GGA are bigger than the experimentally found parameters, but they are close to each other. By taking into account the spin-orbital interaction in the exchange-correlation energy including the density gradient (SGGA), the properties of the $TlInS_2\langle Sn\rangle$ crystals could be correctly described (Tables 1 and 2).

3.1.1. Parameters of the crystal lattice

The optimization of the geometry of the $TlInS_2$ crystal structure with the monoclinic crystal system has shown that the calculation data well agree with the experimental values [7,11] (Table 1). The DFT-calculations for the primitive cell of the polymorphic modification of $TlInS_2$ with the base centered monoclinic crystal system have

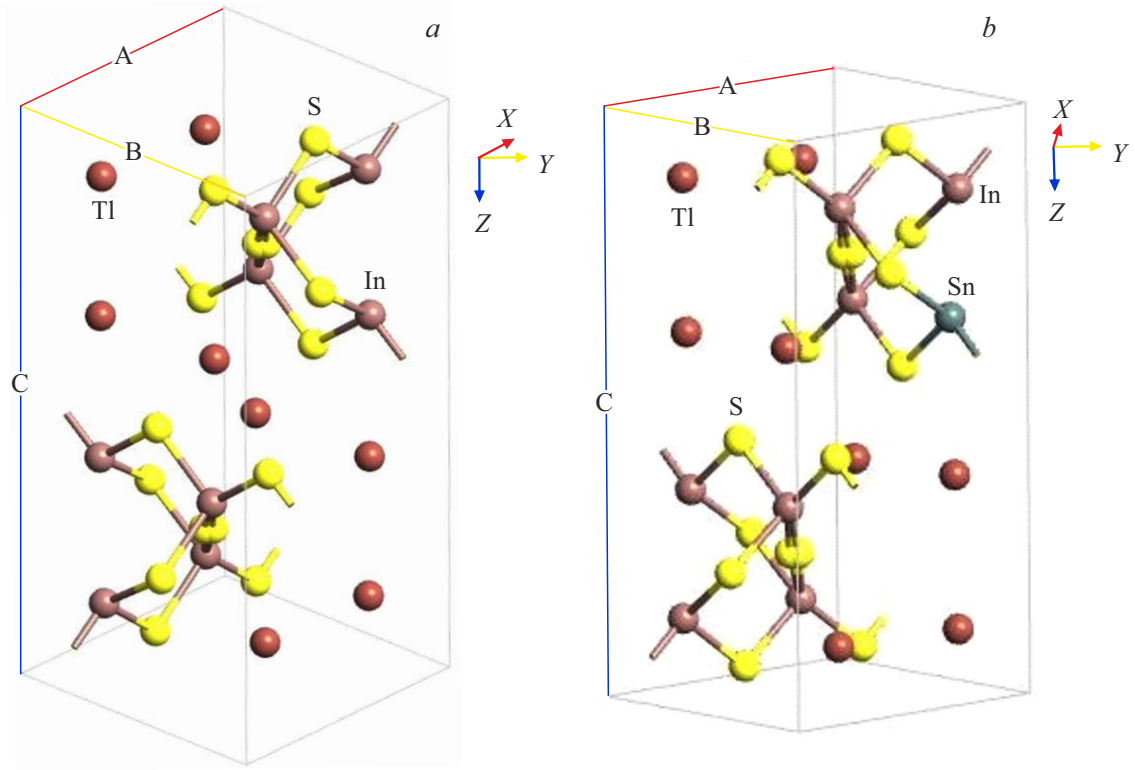

Figure 1. *a* — the primitive cell of the $TlInS_2$ crystal with the monoclinic crystal system (sp.gr. $C2/c$); *b* — the primitive cell of the $TlInS_2\langle Sn\rangle$ crystal with the monoclinic crystal system.

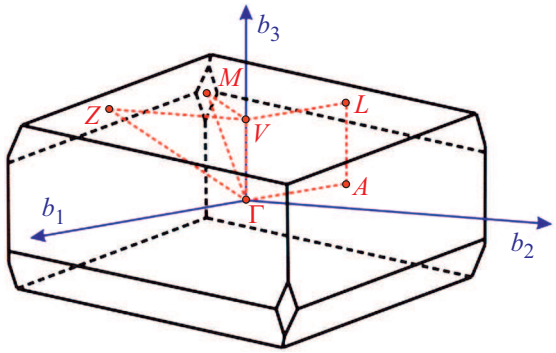

Figure 2. First Brillouin zone of the crystal lattice of the base centered monoclinic crystal system.

shown that it is related to the spatial symmetry group $C2/c$ (C_{2h}^6) and has four formula units for the primitive cell containing 32 atoms. Substitution of indium with a tin atom in the $TlInS_2$ structure does not substantially change parameters of the crystal lattice (Fig. 1, *a, b*).

3.1.2. Band structure

The DFT-calculations show that the $TlInS_2$ cell has a valence band minimum (VBM) and a conductivity band maximum (CBM) in the Γ point of the Brillouin zone (Fig. 2), thereby leading to a direct energetical band gap (E_g). The design $TlInS_2$ band structure is shown in the Fig. 3.

When the In atom is substituted with the Sn atom, the energy gap in the $TlInS_2\langle Sn\rangle$ is reducing, thereby leading to shifting the conductivity band towards the Fermi energy (level) (E_F). Reduction of a range of the energy values, which the electron in the $TlInS_2$ ideal crystal can not have, i.e. of the band gap, is correlated to weakening

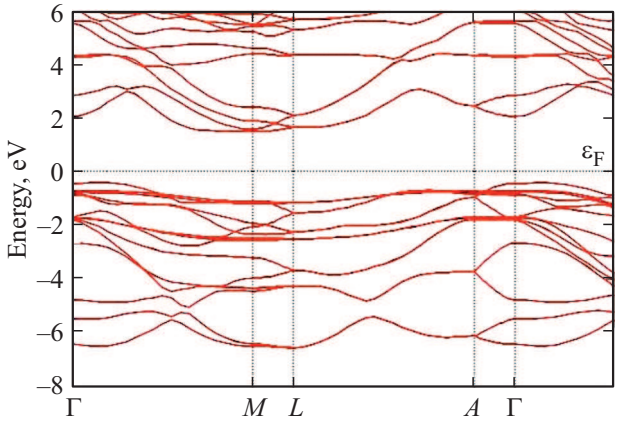

Figure 3. Electron band structure of the $TlInS_2$ crystal with the monoclinic crystal system as calculated by the method of SGGA + *U*.

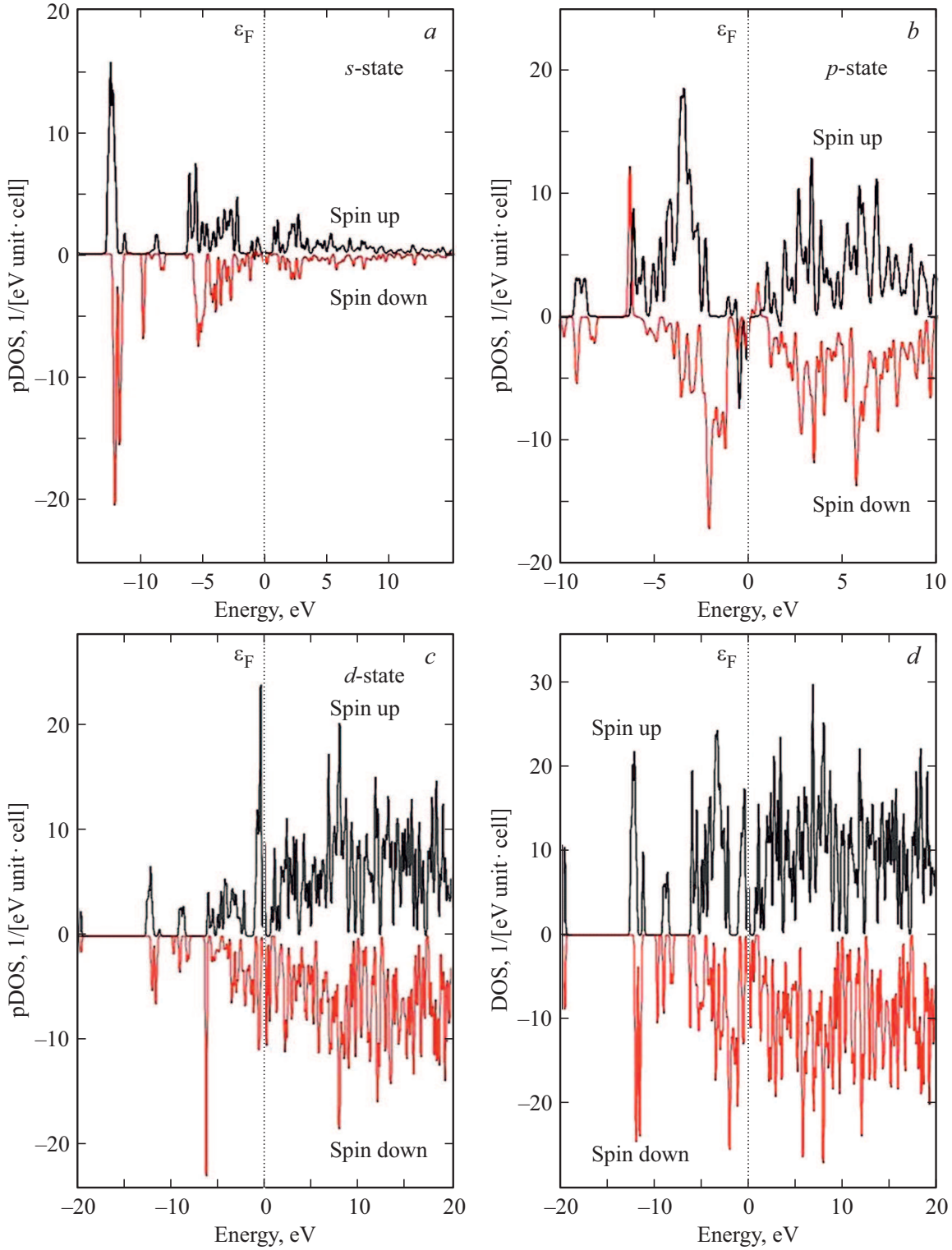

Figure 4. DFT + U-calculated partial densities of the states (pDOS) and the total density of the states (DOS) of the $TlInS_2$ crystal with the spin-up and spin-down. a — s-state, b — p-state, c — d-state, d — total density of the states (DOS).

the chemical bonds in the $TlInS_2\langle Sn\rangle$. It is due to bonding & loosening splitting of the electrons of the atoms of the $TlInS_2\langle Sn\rangle$ components. Using the spin-polarized generalized gradient approximation (SGGA) and taking into account the spin-orbital interaction, we have calculated the band parameters of $TlInS_2\langle Sn\rangle$. The calculated values of the band gap of $TlInS_2$ [24] and $TlInS_2\langle Sn\rangle$ are smaller than the experimental ones [25] (Table 2).

Knowingly [20], the Hubbard model allows describing the interaction of particles in the lattice:

$$H = \sum_{i,j}\sum_{\sigma} T_{ij} c^{+}_{i\sigma} c^{-}_{j\sigma} + \frac{1}{2} I \sum_{\sigma,i} U_i n_{i,\sigma} n_{i,-\sigma} - I \sum_{\sigma,i} \nu_{ii} n_{i\sigma}, \tag{8}$$

where T_{ij} — the transfer integral characterizing electron hops from the i point to the j point; $c^{+}_{i\sigma}$ and $c^{-}_{j\sigma}$ — the operators of creation and annihilation of electrons with the σ spin at the i point; $c^{+}_{i\sigma} c^{-}_{j\sigma} = n_{i,\sigma}$ — the operator of the number of particles with the σ spin at the i point; U_i — the energy of the Coulomb repulsion of two electrons at the i-m point; the integral $I = (ii|1/r|ii)$; $\nu_{ii} = \frac{1}{2} n$.

The calculations of the band gap have taken into account the effects of electron-electron correlations between the atoms. In particular, to amplify the contribution of the p-states of the sulfur atoms to the state density of $TlInS_2\langle Sn\rangle$, the Hubbard parameter was used (U). More exactly, in the calculations the Coulomb repulsion was taken with the energy of $U = 5$ eV. Taking this into account, the obtained values of the band gap of the $TlInS_2$ and $TlInS_2\langle Sn\rangle$ crystals turn out to be close to the values of E_g, which are determined by us from the optical absorption spectra. For example, the band gap $E_g = 2.49$ eV (for $TlInS_2$) has been obtained and it is close to our experimental data ($E_g = 2.539$ eV at 150 K) (Table 2).

The decrease in the band gap of the alloyed $TlInS_2\langle Sn\rangle$ may be correlated to compensation of former active centers with the energy levels of the tin ions. Tin alloying of the $TlInS_2$ single crystal causes intrinsic defects and stimulates flaw migration inside the crystal.

3.1.3. Densities of electron states.

The results of the calculations of the partial density of the states (pDOS) for the $TlInS_2$ crystals are shown in the Fig. 4, *a*–*c*. It follows from the analysis of the partial densities of the states (pDOS) for $TlInS_2$ that the valence band maximum (VBM) is dominated by the p-states of the S ($3p^4$) and Tl ($6p^1$) atoms. At the same time, the conductivity band minimum (CBM) is dominated by the s- and p- states of the In ($5s^2$), S ($3p^4$) atoms and minor contributions by the p-states of the Tl ($6p^1$) and In ($5p^1$) atoms.The $6p^1$-states of the Tl atoms are hybridized with the $6s^2$-state of Tl below the Fermi energy (E_F). Still, the s- and p-states of TI are hybridized with the p-state of In ($5p^1$) atoms below and above E_F.

For the $TlInS_2\langle Sn\rangle$ crystal, the pDOS spectra also indicate small contributions of the s- and p-state of the Sn ($5s^2$) and ($5p^2$) atoms to the density of the states.

3.2. Experimental results

The crystal structure of the polycrystallines and grown single crystals $TlInS_2$ and $TlInS_2\langle 0.1$ mol.% Sn$\rangle$, which is determined by the X-ray powder method, had the monoclinic crystal system with the spatial group $C2/c$ (Fig. 5). The

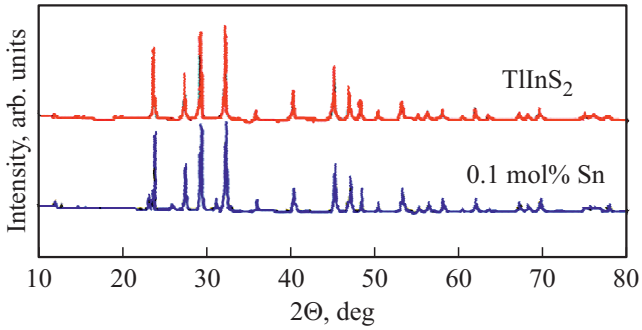

Figure 5. X-ray images of the powders of the single crystal samples of $TlInS_2$ and $TlInS_2\langle 0.1$ mol.% Sn$\rangle$, homogenized at $T = 670$ K.

calculated parameters of the $TlInS_2\langle 0.1$ mol.% Sn$\rangle$ lattice (Table 1) agree with the parameters for the pure $TlInS_2$.

The $TlInS_2\langle Sn\rangle$ single crystal was easily cleaved along the basal plane of the crystal. The tin input into $TlInS_2$ 0.1 mol.% has slightly affected the change of the parameters of the $TlInS_2$ crystal lattice.

3.2.1. Dielectric properties

Let us consider the results of studying the dielectric properties and electric conductivity of the grown $TlInS_2\langle 0.1$ mol.% Sn$\rangle$ single crystal with the monoclinic crystal system, which are measured at the alternating current. The Fig. 6, *a* shows the frequency dependences of the real component of the complex permittivity (ε') of the single crystal samples $TlInS_2\langle Sn\rangle$. It is clear that within all the studied frequency range, the dependence $\varepsilon'(f)$ for $TlInS_2\langle Sn\rangle$ (the curve *2*) is characterized by more sizable dispersion in comparison with $TlInS_2$ (the curve *1*). The tin alloying of the $TlInS_2$ crystal led to noticeable increase in ε' (in 3–4 times). The imaginary part of the complex permittivity (ε'') of the $TlInS_2\langle Sn\rangle$ sample increased even more in comparison with ε'' for $TlInS_2$ (in 11–12 times) (Fig. 6, *b*). In doing so, the tin alloying of $TlInS_2$ led to substantial modification of the curve $\varepsilon''(f)$. If in $TlInS_2$ in all the studied frequency range, there was steady drop ε'', then the curve $\varepsilon''(f)$ for $TlInS_2\langle Sn\rangle$ was characterized by the presence of two maximums at $f = 10^5$ and 10^7 Hz. The frequency dependence of the dielectric losses of $TlInS_2$ is determined not only by the material structure, but the presence of impurities therein and a composition thereof. Similar materials have dielectric losses within the megahertz frequencies, which can be correlated to establishment of the domain polarization.

The experimentally obtained frequency dependence of the dielectric loss tangent (tn
$delta = \varepsilon''/\varepsilon'$) within the $TlInS_2$ sample was of a descending character within the whole studied frequency range (Fig. 6, *c*, the curve *1*). Such a form of the frequency dependence tn δ in the materials corresponds to an electric conductivity loss mechanism. The sample of $TlInS_2\langle Sn\rangle$

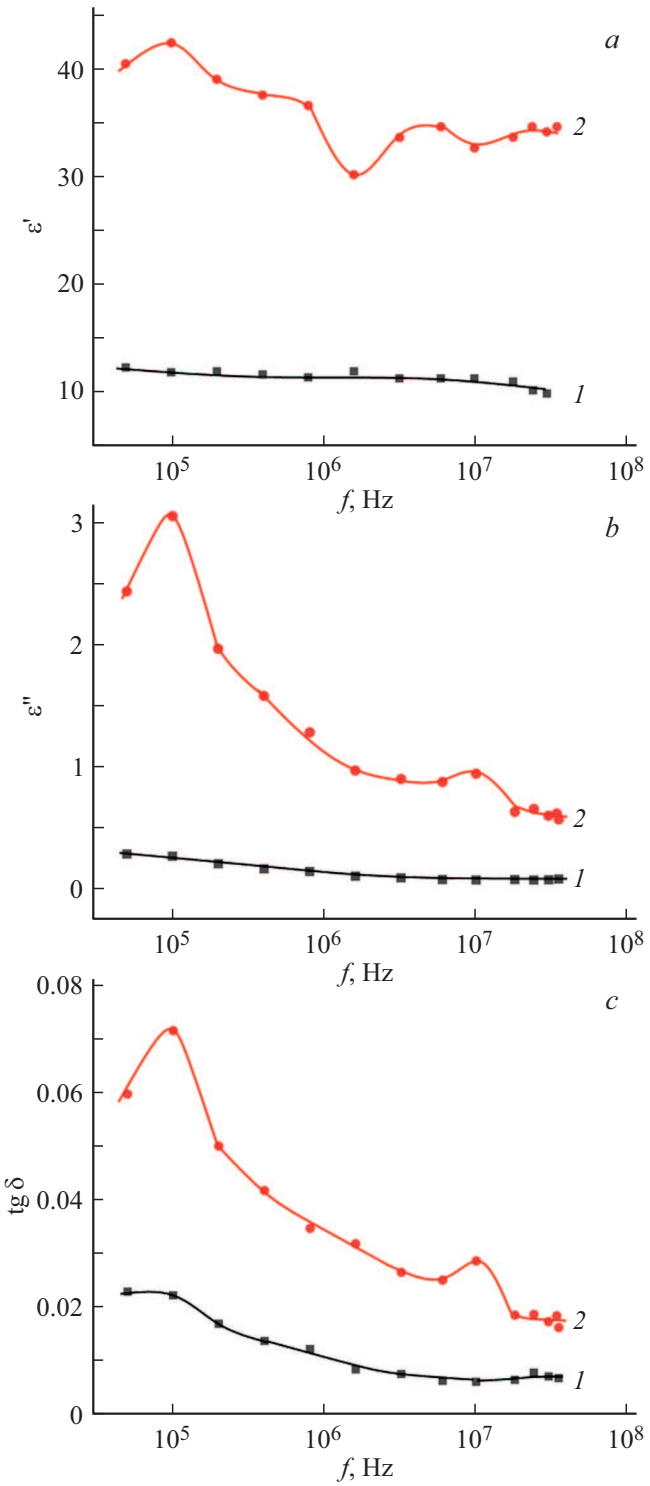

Figure 6. *a* — frequency dependences of the real component of the complex permittivity of the single crystal samples $TlInS_2$ (the curve *1*) and $TlInS_2\langle 0.1\,\text{mol.\% Sn}\rangle$ (the curve *2*); *b* — the frequency dispersion of the imaginary component of the complex permittivity of the single crystal samples $TlInS_2$ (the curve *1*) and $TlInS_2\langle 0.1\,\text{mol.\% Sn}\rangle$ (the curve *2*); *c* — dependences of the dielectric loss tangent on the frequency of the alternating electric field of the single crystal samples $TlInS_2$ (the curve *1*) and $TlInS_2\langle 0.1\,\text{mol.\% Sn}\rangle$ (the curve *2*).

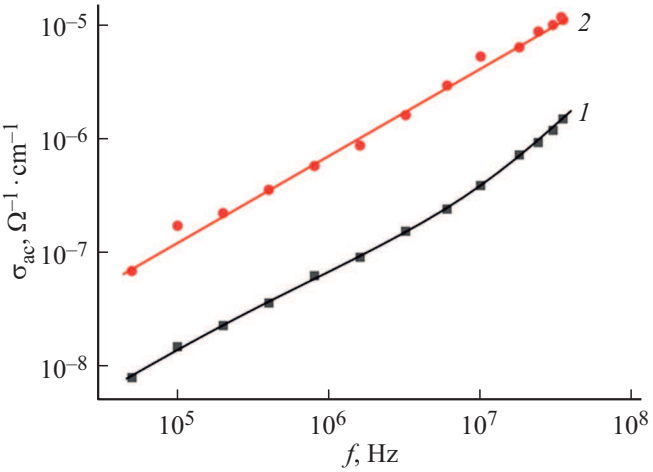

Figure 7. Frequency-dependent ac-conductivity of the single crystal samples of $TlInS_2$ before (the curve *1*) and after (the curve *2*) the alloying 0.1 mol.% Sn.

had relaxation losses, as meant by maximums (Fig. 6, *c*, the curve *2*) at $f = 10^5$ and 10^7 Hz.

3.2.2. Alternating current conductivity (σ_{ac})

The Fig. 7 shows the dependences σ_{ac} for $TlInS_2$ (the curve *1*) and $TlInS_2\langle Sn\rangle$ (the curve *2*). It is established that after inputting the alloying tin into the crystal lattice of the $TlInS_2$ single crystal with the monoclinic crystal system, the conductivity of the samples had increased approximately by one order. For the „pure" $TlInS_2$ single crystal (the curve *1*) within the frequency range $5 \cdot 10^4 - 10^7$ Hz there was a section governed by the dependence $\sigma_{ac} \sim f^{0.8}$, while at $f > 10^7$ Hz there was superlinear dependence $\sigma_{ac} \sim f^{1.2}$. Within the whole studied frequency range, the tin-alloyed $TlInS_2$ single crystals had a regularity $\sigma_{ac} \sim f^{0.8}$.

The dependence $\sigma_{ac} \sim f^{0.8}$ in the materials is typical for a hop conductivity mechanism across local states near the Fermi level [26]:

$$\sigma_{ac}(f) = \frac{\pi^3}{96} e^2 k_B T N_F^2 a_l^5 f \left[\ln\left(\frac{\nu_{ph}}{f}\right)\right]^4, \qquad (9)$$

where e — the electron charge; k_B — the Boltzmann constant; N_F — the density of the states near the Fermi level; $a_l = 1/\alpha$ — the localization radius; α — the constant of the descending wave function of the localized charge carrier $\psi \sim e^{-\alpha r}$; ν_{ph} — the phonon frequency.

As per the formula (9), the ac-conductivity depends on the frequency as $f[\ln(\nu_{ph}/f)]^4$, i.e. at $f \ll \nu_{ph}$ the magnitude α_{ac} is proportional to $f^{0.8}$.

Using the formula (9), the density of the states at the Fermi level was calculated from the experimental values $\alpha_{ac}(f)$ of the sample of $TlInS_2\langle 0.1\,\text{mol.\% Sn}\rangle$. The Table 3 shows the values N_F for pure and tin-alloyed $TlInS_2$ single crystals, as calculated from the electrical alternating-current measurements at 300 K.

Table 3. Calculated parameters of the localized states in the single crystals of $TlInS_2$ and $TlInS_2\langle 0.1\,mol.\%\,Sn\rangle$ with the monoclinic crystal system at 300 K

Composition	N_F, $eV^{-1}\cdot cm^{-3}$	τ, s	R, Å	ΔE, eV	N_t, cm^{-3}
$TlInS_2$	$5.2\cdot 10^{18}$	$2\cdot 10^{-7}$	86	0.14	$7.3\cdot 10^{17}$
$TlInS_2\langle Sn\rangle$	$1.7\cdot 10^{19}$	$5.9\cdot 10^{-8}$	77	0.06	10^{18}

At the calculated N_F, the value σ_{ph} is taken to be equal to 10^{12} Hz, while the localization radius is taken to be our experimental value $a_l = 14$ Å [1].

According to the alternating current hopping conductivity, the average hop distance (R) is determined using the following formula:

$$R = \frac{1}{2\alpha}\ln\left(\frac{\nu_{ph}}{f}\right). \qquad (10)$$

The Table 3 shows the values R, calculated by the formula (10), for the $TlInS_2$ and $TlInS_2\langle Sn\rangle$ crystals, too. These values R exceed in 5.5–6 times the average distance between the localization centers of the charge carries in $TlInS_2$. Using the R values calculated as follows:

$$\tau^{-1} = \nu_{ph}\exp(-2\alpha R) \qquad (11)$$

we determined the average hop time in the studied crystals (the 3d column of the Table 3).

Using the formula from [26]:

$$\Delta E = 3/2\pi R^3\cdot N_F \qquad (12)$$

for the $TlInS_2$ and $TlInS_2\langle Sn\rangle$ single crystals were evaluated the energy scattering of the states localized near the Fermi level (ΔE). These values are given in the fifth column of the Table 3.

Using the formula:

$$N_t = N_F\cdot\Delta E \qquad (13)$$

we have determined a concentration of deep traps (N_t) accounted for ac-conductivity in the $TlInS_2$ and $TlInS_2\langle Sn\rangle$ single crystals (the last column of the Table 3).

As it is clear from the Table 3, with addition of tin to $TlInS_2$ with the monoclinic crystal system, the density of states localized near the Fermi level increases, whereas the time and distance of hops decrease as compared to $TlInS_2$. It seems to be happening due to a narrower energy band of the localized states (ΔE) in $TlInS_2$ approximately in two times. At this, the concentration of the charge carrier at the deep levels in $TlInS_2\langle Sn\rangle$ insignificantly increases in comparison with N_t in $TlInS_2$. Thus, it is established that inputting tin into the crystal lattice of the $TlInS_2$ modified the frequency dependences of its dielectric coefficients and parameters of the states localized in the band gap.

3.2.3. Optical absorption edge

The temperature range 150–300 K was studied for the optical absorption edge of the $TlInS_2$ and $TlInS_2\langle 0.1\,mol.\%\,Sn\rangle$ single crystal samples. The optical absorption coefficient (α) within the range from 1 to 10^5 cm^{-1} was calculated by using measurement data of the intensity of the light beam, which passed through the samples of various thicknesses. In order to cover the whole wave length range, it was divided into three sections to take into account results of transmission measurement of three sample pairs of $TlInS_2$ and $TlInS_2\langle 0.1\,mol.\%\,Sn\rangle$ of the corresponding thicknesses. For each wave length section, the absorption coefficient was calculated by the formula:

$$\alpha = 1/(d_2 - d_1)\cdot\ln(I_1/I_2), \qquad (14)$$

where d_1 and d_2 — the thicknesses of the single crystal samples, I_1 and I_2 — the intensities of light passed through the single crystal samples. The value αd was higher than one for each sample and the corresponding section. That is why there was insignificant interference of light beams, which was passed and reflected from the rear surface of the single crystal samples.

The ternary compound of $TlInS_2$ with the monoclinic crystal system is a semiconductor with a direct interband transition. The band gap E_g was determined by extrapolation of a straight section of the dependence $(\alpha h\nu)^2$ on the photon energy $h\nu$ to the intersection with the abscissa axis. The transmission spectra obtained allowed determining the temperature dependence of the band gap of the $TlInS_2\langle Sn\rangle$ crystals within the temperature range from 150 to 300 K.

The Fig. 8 shows the dependence $E_g(T)$ for the single crystal samples of $TlInS_2$ and $TlInS_2\langle Sn\rangle$. It is established

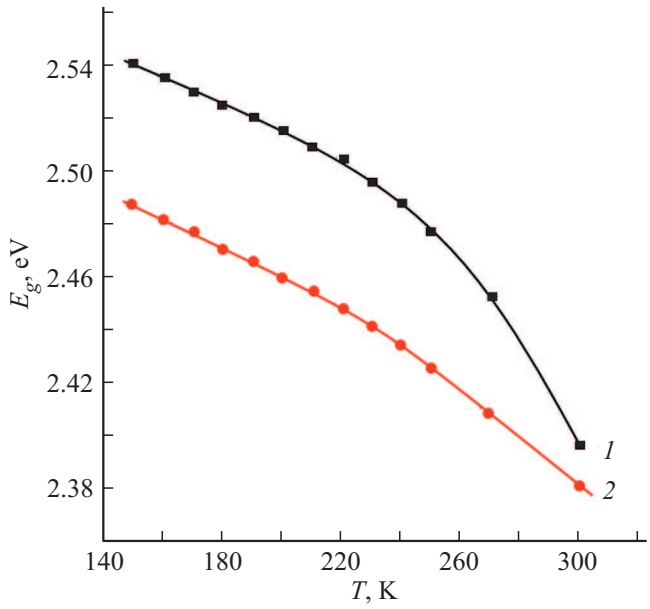

Figure 8. Temperature dependence of the band gap of the single crystal samples of $TlInS_2$ (the curve *1*) and $TlInS_2\langle 0.1\,mol.\%\,Sn\rangle$ (the curve *2*).

that with decrease in the temperature, the sample's absorption edge is shifting towards the high energies. The average temperature coefficient of the band gap $\partial E_g/\partial T$ was calculated for $TlInS_2\langle Sn\rangle$ within the temperature range of 150–300 K. The value $\partial E_g/\partial T$ has a negative sign both for $TlInS_2$ and for $TlInS_2\langle Sn\rangle$ ($-9.5\cdot10^{-4}$ eV/K for $TlInS_2$ and $-7\cdot10^{-4}$ eV/K for $TlInS_2\langle Sn\rangle$). The band gap of the $TlInS_2\langle Sn\rangle$ single crystal in comparison with E_g of the pure $TlInS_2$ is decreasing to by 16 meV at 300 K and 53 meV at 150 K. That is, tin alloying of the $TlInS_2$ single crystals with the quantity of 0.1 mol.% significantly reduces the band gap of $TlInS_2\langle Sn\rangle$. The reduction of E_g may be caused, in particular, by increase in the flaw concentration when increasing the concentration of the tin alloying impurity.

4. Conclusion

Thus, from the electron properties of the supercells of the $TlInS_2$ and $TlInS_2\langle Sn\rangle$ crystals with the monoclinic crystal system, with ab initio calculation, the following can be deduced. From the distribution of the density of the electron states it follows that the top of the valence band is made of the $3p$-states of sulfur, and the bottom of the conductivity band is made of the p-states of all the $TlInS_2$ atoms, the contribution of the $5s^2$-states of In and an impurity of the $5s^2$-states of Sn. The deepest subband in the valence band from -16 eV to 0 eV is made of the $4d$-states of indium (-16; -14 eV). The next energy range from -12 to -7.5 eV consists in the $3s$-states of sulfur and the $5d$-states of thallium. The range from -7 to -5 eV consists in the $3p$-states of S and the s-states of atoms of In ($5s^2$) and Tl ($6s^2$). The energy band between -5 and 0 eV is correlated to the contribution of the $3p$-states of S, hybridized with the p-states of ($5p^1$) indium atoms and ($6p^1$) atoms.

Taking into account the Hubbard model, the DFT-estimated values of the band gap (E_g) of the $TlInS_2\langle Sn\rangle$ crystals turn out to be close to the values of E_g (2.17 eV; SGGA-PBE), which are determined from the optical adsorption spectra (2.383 eV at $T = 300$ K). The reduction of E_g of the $TlInS_2\langle Sn\rangle$ crystal in comparison with $TlInS_2$ (2.49 eV; SGGA-PBE) may be due to increase in the flaw concentration when increasing the tin alloying impurity concentration in the crystal lattice.

The dielectric and optical measurements of the $TlInS_2$ and $TlInS_2\langle 0.1\,\text{mol.\% Sn}\rangle$ homogeneous single crystals (which were grown by the directional crystallization) with the monoclinic crystal system allow concluding as follows. There is evident significant frequency dispersion of the real and imaginary components of the complex permittivity and conductivity of the $TlInS_2\langle Sn\rangle$ single crystals at $f = 5\cdot10^4$–$3.5\cdot10^7$ Hz. A nature of the dielectric losses (relaxation losses) and the hopping charge transfer mechanism in $TlInS_2\langle Sn\rangle$ have been ascertained. Inputting tin into the $TlInS_2$ crystal lattice leads to the increase in real (in 3–4 times) and imaginary (in 11–12 times) components of their complex permittivity and dielectric loss tangent. Besides, the conductivity of the $TlInS_2\langle 0.1\,\text{mol.\% Sn}\rangle$ single crystals at the alternating current (σ_{ac}) also increases by one order. Based on the results of the electric measurements at the alternating current at 300 K, the calculated parameters of the localized states in $TlInS_2\langle Sn\rangle$ have the following values: the density of the states near the Fermi level $N_F = 1.7\cdot10^{19}\,\text{eV}^{-1}\cdot\text{cm}^{-3}$ and their energy scattering $\Delta E = 0.06$ eV, the average time $\tau = 5.9\cdot10^{-8}$ s and the hopping distance $R = 77$ Å, the concentration of deep traps $N_t = 10^{18}\,\text{cm}^{-3}$. In comparison with the $TlInS_2$ pure single crystal, inputting tin into the $TlInS_2$ structure was leading to decrease in the average distance and the hopping time, as well as to increase in the density of states localized near the Fermi level in the band gap.

The experimentally obtained dependences were used to calculate the absorption spectra and determine the optical band gap of the $TlInS_2$ and $TlInS_2\langle Sn\rangle$ single crystals. It is established that with temperature decrease, the optical absorption edge of the $TlInS_2\langle Sn\rangle$ single crystal is shifting towards the high energies. The calculated average temperature coefficient of the band gap is: $\partial E_g/\partial T = -7\cdot10^{-4}$ eV/K for $TlInS_2\langle Sn\rangle$ within the temperature range of 150–300 K. The band gap of the $TlInS_2\langle Sn\rangle$ (2.383 eV at 300 K) single crystal decreases in comparison with the pure $TlInS_2$ single crystal (2.399 eV at 300 K). In particular, such decrease in E_g is 53 meV at 150 K and 16 meV at 300 K.

Funding

This study was in part supported by the Science Development Fund under the President of the Republic of Azerbaijan, project E.F-BGM-4-RFTF-1/2017-21/05/1-M-07 and the Russian Foundation for Basic Research, project 18-57-06001 no. Az_a 2018.

Conflict of interest

The authors declare that they have no conflict of interest.

References

[1] S.N. Mustafaeva, M.M. Asadov, A.A. Ismailov. Phys. Solid State **51**, *11*, 2269 (2009). https://doi.org/10.1134/S1063783409110122.
[2] O.B. Plusch, A.Yu. Sheleg. Kristallografiya **44**, *5*, 873 (1999) (in Russian). https://doi.org/10.1134/1.171106
[3] S.N. Mustafaeva, E.M. Kerimova, D.A. Guseinova. Phys. Status Solidi A **179**, 199 (2000). https://doi.org/10.1002/1521-396X(200005)179:1¡199::AID-PSSA199¿3.0.CO;2-W
[4] K.R. Allakhverdiev, N.D. Akhmed-zade, T.G. Mamedov, T.S. Mamedov, Mir-Gasan Yu. Seidov. Low Temp. Phys. **26**, *1*, 56 (2000). https://doi.org/10.1063/1.593863
[5] K.R. Allakhverdiev, T.G. Mammadov, R.A. Suleymanov, N.Z. Gasanov. J. Phys.: Condens. Matter **15**, 1291 (2003). https://doi.org/10.1088/0953-8984/15/8/313
[6] A.F. Qasrawi, N.M. Gasanly. J. Mater. Sci. **41**, 3569 (2006). https://doi.org/10.1007/s10853-005-5618-0

[7] W. Henkel, H.D. Hochheimer, C. Carlone, A. Werner, S. Ves, H.G.v. Schnering. Phys. Rev. B **26**, *6*, 3211 (1982). https://doi.org/10.1103/PhysRevB.26.3211
[8] H. Hahn, B. Wellman. Naturwis. **54**, *2*, 42 (1967). https://doi.org/10.1007/bf00680166
[9] T.J. Isaacs, J.D. Feichtner. J. Solid State Chem. **14**, *3*, 260 (1975). https://doi.org/10.1016/0022-4596(75)90030-4
[10] K.-J. Range, G. Engert, W.A. Muller, A. Weiss. Z. Naturforsch. B **29**, 181 (1974). https://doi.org/10.1515/znb-1974-3-410
[11] S. Kashida, Y. Kobayashi. J. Phys.: Condens. Matter **11**, *4*, 1027 (1999). https://doi.org/10.1088/0953-8984/11/4/010
[12] S.N. Mustafaeva, M.M. Asadov. Physics of the Solid State **40**, *4*, 612 (1998).
[13] A.U. Sheleg, V.V. Shautsova, V.G. Hurtavy, S.N. Mustafaeva. J. Surf. Invest.: X-Ray, Synchrotron and Neutron Techniques **7**, *6*, 1052 (2013). https://doi.org/10.1134/s1027451013060190.
[14] M. Isik, N.M. Gasanly, F. Korkmaz. Phys. B: Condens. Matter **421**, 50 (2013). https://doi.org/10.1016/j.physb.2013.03.046
[15] S.N. Mustafaeva, M.M. Asadov, V.A. Ramazanzade. Physics of the Solid State **38**, *1*, 14 (1996).
[16] S. Kazan, M. Açikgöz, F.A. Mikailov, T. Mammadov, B. Aktaş. Ph. Transit **81**, *6*, 581 (2008). https://doi.org/10.1080/01411590802017476
[17] T. Babuka, O.O. Gomonnai, K.E. Glukhov, L.Yu. Kharkhalis, A.V. Gomonnai, M. Makowska-Janusik. Low Temp. Phys. **48**, 57 (2022). https://doi.org/10.1063/10.0008965
[18] M.M. Asadov, S.N. Mustafaeva, S.S. Guseinova, V.F. Lukichev, D.B. Tagiev. Phys. Solid State **63**, *5*, 797 (2021). https://doi.org/10.1134/S1063783421050036.
[19] S.N. Mustafaeva, M.M. Asadov, S.S. Guseinova, V.F. Lukichev, D.B. Tagiev. Physics of the Solid State **64**, *1*, 46 (2022). https://doi.org/10.21883/FTT.2022.01.51830.182.
[20] S.N. Mustafaeva, M.M. Asadov, S.S. Guseinova, A.I. Dzhabarov, V.F. Lukichev. Physics of the Solid State **64**, *4*, 428 (2022). https://doi.org/10.21883/FTT.2022.04.52182.251
[21] M.M. Asadov, S.N. Mustafaeva, S.S. Guseinova, V.F. Lukichev. Physics of the Solid State **64**, *5*, 528 (2022). https://doi.org/10.21883/FTT.2022.05.52332.270
[22] S.N. Mustafaeva, M.M. Asadov, E.M. Kerimova, N.Z. Gasanov. Inorg. Mater. **49**, *12*, 1175 (2013). https://doi.org/10.1134/S0020168518070099
[23] M.M. Asadov, S.N. Mustafaeva, S.S. Guseinova, V.F. Lukichev. Mikroelektronika **51**, *2*, 125 (2022) (in Russian). https://doi.org/10.31857/S0544126922010021
[24] T. Babuka, O.O. Gomonnai, K.E. Glukhov, L.Yu. Kharkhalis, M. Sznajder, D.R.T. Zahn. Acta Phys. Pol. A **136**, *4*, 640 (2019). https://doi.org/10.12693/APhysPolA.136.640
[25] O.V. Korolik, S.A. Kaabi, K. Gulbinas, A.V. Mazanik, N.A. Drozdov, V. Grivickas. J. Lumin. **187**, 507 (2017). https://doi.org/10.1016/j.jlumin.2017.03.065
[26] N.F. Mott, E.A. Davis. Electronic Processes in Non-Crystalline Materials. OUP Oxford (2012). 590 p. ISBN: 9780199645336